

Large basis *ab initio* shell model investigation of ${}^9\text{Be}$ and ${}^{11}\text{Be}$

C. Forssén,* P. Navrátil, and W.E. Ormand

Lawrence Livermore National Laboratory, P.O. Box 808, L-414, Livermore, CA 94551

E. Caurier

*Institut de Recherches Subatomiques (IN2P3-CNRS-Université Louis Pasteur)
Batiment 27/1, 67037 Strasbourg Cedex 2, France*

(Dated: July 18, 2018)

We are presenting the first *ab initio* structure investigation of the loosely bound ${}^{11}\text{Be}$ nucleus, together with a study of the lighter isotope ${}^9\text{Be}$. The nuclear structure of these isotopes is particularly interesting due to the appearance of a parity-inverted ground state in ${}^{11}\text{Be}$. Our study is performed in the framework of the *ab initio* no-core shell model. Results obtained using four different, high-precision two-nucleon interactions, in model spaces up to $9\hbar\Omega$, are shown. For both nuclei, and all potentials, we reach convergence in the level ordering of positive- and negative-parity spectra separately. Concerning their relative position, the positive-parity states are always too high in excitation energy, but a fast drop with respect to the negative-parity spectrum is observed when the model space is increased. This behavior is most dramatic for ${}^{11}\text{Be}$. In the largest model space we were able to reach, the $1/2^+$ level has dropped down to become either the first or the second excited state, depending on which interaction we use. We also observe a contrasting behavior in the convergence patterns for different two-nucleon potentials, and argue that a three-nucleon interaction is needed to explain the parity inversion. Furthermore, large-basis calculations of ${}^{13}\text{C}$ and ${}^{11}\text{B}$ are performed. This allows us to study the systematics of the position of the first unnatural-parity state in the $N = 7$ isotone and the $A = 11$ isobar. The ${}^{11}\text{B}$ run in the $9\hbar\Omega$ model space involves a matrix with dimension exceeding 1.1×10^9 , and is our largest calculation so far. We present results on binding energies, excitation spectra, level configurations, radii, electromagnetic observables, and ${}^{10}\text{Be} + n$ overlap functions.

PACS numbers: 21.60.Cs, 21.45.+v, 21.30.-x, 21.30.Fe, 27.20.+n

I. INTRODUCTION

Studies of how nuclear structure evolves when varying the N/Z ratio are important in order to improve our fundamental understanding of nuclear forces. For this reason, research on light neutron-rich nuclei has attracted an increasing amount of theoretical and experimental effort since the advent of radioactive nuclear beams. The application of a standard mean-field picture to describe these few-body systems is questionable, and it is not surprising that substantial deviations from regular shell structure has been observed. The $A = 11$ isobar is of particular interest in this respect since it exhibits some anomalous features that are not easily explained in a simple shell-model framework. Most importantly, the parity-inverted $1/2^+$ ground state of ${}^{11}\text{Be}$ was noticed by Talmi and Unna [1] already in the early 1960s, and it still remains one of the best examples of the disappearance of the $N = 8$ magic number.

Many theoretical studies of odd- A beryllium isotopes have already been performed using various models. A thorough review of the structure of unstable light nuclei in terms of the shell model can be found in Ref. [2]. Of particular interest is the study on unnatural-parity states of the $A = 11$ isobar by Teeters and Kurath [3] us-

ing a $1\hbar\Omega$ model space and the Millener-Kurath interaction with modified $0s$ and sd single-particle energies. The halo structure of the ${}^{11}\text{Be}$ ground state was reproduced with the variational shell model by Otsuka *et al* [4]. They used Skyrme interactions and constructed multi-nucleon wave functions from a variational single-particle basis in a $(0-1)\hbar\Omega$ model space. Alternatively, the loosely-bound nature of the valence neutron in ${}^{11}\text{Be}$ can be treated explicitly in a ${}^{10}\text{Be} + n$ picture with a Woods-Saxon potential, see e.g. Refs. [5, 6]. Using a coupled-channels treatment, the authors of these papers found a significant overlap with excited-core states. Possible explanations for the parity inversion of the ${}^{11}\text{Be}$ ground state has also been investigated using the AMD+HF model [7], which is a combination of anti-symmetrized molecular dynamics with the concept of single-particle motion. An extended version of the AMD framework was later used to study excited states of ${}^{11}\text{Be}$, and the existence of three negative-parity rotational bands was proposed [8].

There are also several calculations involving different cluster models. In particular, α -clustering has been considered to play an important role in these systems. With this assumption as a starting point, K. Arai *et al* used an $\alpha + \alpha + n$ model and obtained the ground state of ${}^9\text{Be}$ using the stochastic variational method, while several particle-unbound excited states were studied simultaneously with the complex scaling method [9]. A similar $\alpha + \alpha + Xn$ description was employed by P. Descouvemont [10] in his study of possible rotational bands in

*c.forssen@llnl.gov

${}^9\text{-}^{11}\text{Be}$ using the Generator Coordinate Method. His conclusion, however, was that the degree of α -clustering decreased with increasing mass, and consequently his model was not able to reproduce some of the anomalous properties of ${}^{11}\text{Be}$.

Unfortunately, due to the complexity of the problem, there has been no genuine *ab initio* investigation of ${}^{11}\text{Be}$ starting from realistic inter-nucleon interactions. There is no doubt that the cluster and potential models are very successful, and can provide reasonable explanations for many observations. Still, one has to remember that they rely upon the fundamental approximation that the total wave function can be separated into cluster components. Furthermore, the effective interactions used in all models must be fitted to some observables for each individual case. On the contrary, a truly microscopic theory such as the Green's Function Monte Carlo (GFMC) method [11], or the *ab initio* no-core shell model (NCSM) [12, 13], starts from a realistic inter-nucleon potential and solves the A -body problem, producing an antisymmetrized total wave function. It is a true challenge of our understanding of atomic nuclei to investigate nuclear many-body systems ($A > 4$) using such *ab initio* approaches.

This paper represents an effort to fill this gap. Our study is performed in the framework of the *ab initio* NCSM, in which the A -body Schrödinger equation is solved using a large Slater determinant harmonic oscillator (HO) basis. However, it is well known that the HO basis functions have incorrect asymptotics which might be a problem when trying to describe loosely bound systems. Therefore it is desirable to include as many terms as possible in the expansion of the total wave function. By restricting our study to two-nucleon (NN) interactions, even though the NCSM allows for the inclusion of three-body forces, we are able to maximize the model space and to better observe the convergence of our results.

In Sec. II the framework for the NCSM will be briefly outlined, and the four different high-precision NN interactions that are used in this work will be introduced. Sec. III is devoted to a presentation and discussion of our complete set of results for ${}^9,{}^{11}\text{Be}$, with a particular focus on the position of the first unnatural-parity state. Concluding remarks are presented in Sec. IV.

II. AB INITIO NO-CORE SHELL MODEL

Applying the *ab initio* NCSM is a multi-step process. The first step is to derive the effective interaction from the underlying inter-nucleon forces, and to transform it from relative coordinates into the single-particle M -scheme basis. The second step is to evaluate and diagonalize the effective Hamiltonian in an A -nucleon (Z protons and N neutrons) Slater determinant HO basis that spans the complete $N_{\max}\hbar\Omega$ model space. Finally, we can use the resulting wave functions for further processing. This section contains a short discussion on each

of these steps. We stress that an important strength of the method is the possibility to include virtually any type of inter-nucleon potential. The four high-precision NN interactions that have been used in this study will be introduced in Sec. II C. A more detailed description of the NCSM approach, as it is implemented in this study, can be found in, e.g., Ref. [13].

A. Hamiltonian and effective interactions

The goal is to solve the A -body Schrödinger equation with an intrinsic Hamiltonian of the form

$$H_A = \frac{1}{A} \sum_{i < j}^A \frac{(\vec{p}_i - \vec{p}_j)^2}{2m} + \sum_{i < j}^A V_{NN,ij}, \quad (1)$$

where m is the nucleon mass and $V_{NN,ij}$ is the NN interaction including both strong and electromagnetic components. As mentioned earlier, we will not use three-body forces in this study since we strive to maximize the size of the model space. By adding a center-of-mass (CM) HO Hamiltonian $H_{\text{CM}}^\Omega = T_{\text{CM}} + U_{\text{CM}}^\Omega$ (where $U_{\text{CM}}^\Omega = Am\Omega^2 \vec{R}^2/2$, $\vec{R} = \sum_{i=1}^A \vec{r}_i/A$), we facilitate the use of a convenient HO basis. The modified Hamiltonian can be separated into one- and two-body terms

$$\begin{aligned} H_A^\Omega &= H_A + H_{\text{CM}}^\Omega = \sum_{i=1}^A h_i + \sum_{i < j}^A V_{ij}^{\Omega,A} \\ &= \sum_{i=1}^A \left[\frac{\vec{p}_i^2}{2m} + \frac{1}{2} m\Omega^2 \vec{r}_i^2 \right] \\ &\quad + \sum_{i < j}^A \left[V_{NN,ij} - \frac{m\Omega^2}{2A} (\vec{r}_i - \vec{r}_j)^2 \right]. \end{aligned} \quad (2)$$

The next step is to divide the A -nucleon infinite HO basis space into an active, finite model space (P) and an excluded space ($Q = 1 - P$). The model space consists of all configurations with $\leq N_{\max}\hbar\Omega$ excitations above the unperturbed ground state. In this approach there is no closed-shell core; meaning that all nucleons are active.

Since we solve the many-body problem in a finite model space, the realistic NN interaction will yield pathological results because of the short-range repulsion. Consequently, we employ effective interaction theory. In the *ab initio* NCSM approach, the model-space dependent effective interaction is constructed by performing a unitary transformation of the Hamiltonian (2), $e^{-S} H_A^\Omega e^S$, such that the model space and the excluded space are decoupled $Q e^{-S} H_A^\Omega e^S P = 0$. This procedure has been discussed by Lee and Suzuki [14, 15], and yields a Hermitian effective interaction $H_{\text{eff}} = P e^{-S} H_A^\Omega e^S P$ which acts in the model space and reproduces exactly a subset of the eigenspectrum to the full-space Hamiltonian. In general, this effective Hamiltonian will be an A -body operator which is essentially as difficult to construct as to solve the

full A -body problem. In this study we approximate the effective Hamiltonian at the two-body cluster level. The basic idea is to derive it from high-precision solutions to the two-body problem with $\mathcal{H}_2 = h_1 + h_2 + V_{12}^{\Omega,A}$, where the two-body term is the same as in Eq. (2). The final result will be a two-body effective interaction $V_{12,\text{eff}}^{\Omega,A}$. See Ref. [13, 16] for details.

We note that our approximated effective interaction will depend on the nucleon number A , the HO frequency Ω , and the size of the model space which is defined by N_{max} . However, by construction, it will approach the starting bare interaction $V_{ij,\text{eff}}^{\Omega,A} \rightarrow V_{ij}^{\Omega,A}$, as $N_{\text{max}} \rightarrow \infty$. Consequently, the dependence on Ω will decrease with increasing model space, and the NCSM results will converge to the exact solution. A very important feature of the NCSM is the fact that the effective interaction is translationally invariant so that the solutions can be factorized into a CM component times a wave function corresponding to the internal degrees of freedom. Due to this property it is straightforward to remove CM effects completely from all observables.

B. Solution of the many-body Schrödinger equation

Once the effective interaction has been derived, we can construct the effective Hamiltonian in the A -body space. In this process we subtract the CM Hamiltonian H_{CM}^{Ω} , and add the Lawson projection term $\beta(H_{\text{CM}} - \frac{3}{2}\hbar\Omega)$ to shift eigenstates with excited CM motion up to high energies. States with 0S CM motion are not affected by this term and, consequently, their eigenenergies will be independent of the particular choice of β . We are now left with a Hamiltonian of the form

$$H_{A,\text{eff}}^{\Omega} = P \left\{ \sum_{i<j}^A \left[\frac{(\vec{p}_i - \vec{p}_j)^2}{2Am} + \frac{m\Omega^2}{2A}(\vec{r}_i - \vec{r}_j)^2 + V_{ij,\text{eff}}^{\Omega,A} \right] + \beta \left(H_{\text{CM}} - \frac{3}{2}\hbar\Omega \right) \right\} P. \quad (3)$$

The computational problem of obtaining the many-body eigenvalues is non-trivial due to the very large matrix dimensions involved. The largest model space that we encountered in this study was the ^{11}B $9\hbar\Omega$ (positive parity) space, for which the dimension exceeds $d_P = 1.1 \times 10^9$. For ^{11}Be (^9Be), the $9\hbar\Omega$ space gives $d_P = 7.1 \times 10^8$ (2.0×10^8). To solve this problem we have used a specialized version of the shell model code ANTOINE [17, 18], recently adapted to the NCSM [19]. This code works in the M scheme for basis states, and uses the Lanczos algorithm for diagonalization. The number of iterations needed to converge the first eigenstates is significantly reduced by the implementation of a sophisticated strategy for selecting the pivot vectors. This feature of the code is absolutely crucial when using it to perform calculations in very large model spaces.

Furthermore, the code takes advantage of the fact that the dimensions of the neutron and proton spaces are small with respect to the full dimension. Therefore, before the diagonalization, all the matrix elements involving one- and two-body operators acting in a single subspace (proton or neutron) are calculated and stored. As a consequence, during the Lanczos procedure, all non-zero proton-proton and neutron-neutron matrix elements can be generated with a simple loop. Furthermore, the proton-neutron matrix elements are obtained with three integer additions [17]. However, for no-core calculations (in which all nucleons are active) the number of shells and, consequently, the number of matrix elements that are precalculated, becomes very large. Consider, e.g., the ^{11}B calculation in the $9\hbar\Omega$ space. The full dimension is $d_P = 1.1 \times 10^9$, while the number of active shells is 66 and the total number of neutron plus proton Slater determinants is $N(n) + N(p) = 1.0 \times 10^7$. This corresponds to 80 Gb of precalculated and stored matrix elements. In contrast, consider a shell-model calculation of ^{57}Ni in the full fp space. The total dimension is larger, $d_P = 1.4 \times 10^9$, but there are only four active shells which gives $N(n) + N(p) = 1.8 \times 10^6$ and requires merely 1 Gb of precalculated data.

A recent development of the NCSM is the ability to further process the wave functions, resulting from the shell-model calculation, to obtain translationally invariant densities [20] and cluster form factors [21]. The latter can be used to obtain spectroscopic factors, but can also serve as a starting point for an *ab initio* description of low-energy nuclear reactions. We have employed these new capabilities to study the overlap of ^{11}Be with different $^{10}\text{Be} + n$ channels.

C. Realistic NN interactions

Four different, high-precision NN interactions have been used in this study. These are: the Argonne V8' (AV8') [11, 22], the CD-Bonn 2000 (CDB2k) [23], the N³LO [24], and the INOY [25, 26] potentials. We can divide these interactions into three different types:

1. *Local in coordinate space*: The AV8' interaction is an isospin-invariant subset of the phenomenological Argonne v_{18} potential [22] plus a screened Coulomb potential. This interaction is local in coordinate space and it is also employed in the Green's Function Monte Carlo (GFMC) approach [11]. Consequently, the use of this potential allows for a direct comparison of results from the NCSM and the GFMC methods.

2. *Non-Local in momentum space*: The CDB2k interaction [23] is a charge-dependent NN interaction based on one-boson exchange. It is described in terms of covariant Feynman amplitudes, which are non-local. Consequently, the off-shell behavior of the CD-Bonn interaction differs from commonly used local potentials which leads to larger binding energies in nuclear few-body systems. The newly developed N³LO interaction [24] is also rep-

resented by a finite number of Feynman diagrams. This interaction, however, is based on chiral perturbation theory at the fourth order, which means that it is derived from a Lagrangian that is consistent with the symmetries of QCD. It represents a novel development in the theory of nuclear forces. It is particularly interesting to note that many-body forces appear naturally already at the next-to-next-to-leading order (NNLO) of this low-energy expansion. However, in this study we use solely the NN part of the $N^3\text{LO}$ interaction. This NN potential has previously been applied in the NCSM approach to study the p -shell nuclei ${}^6\text{Li}$ and ${}^{10}\text{B}$ [27].

3. *Non-Local in coordinate space:* A new type of interaction, which respects the local behavior of traditional NN interactions at longer ranges but exhibits a non-locality at shorter distances, was recently proposed by Doleschall *et al* [25, 26]. The authors are exploring the extent to which effects of multi-nucleon forces can be absorbed by non-local terms in the NN interaction. Their goal was to investigate if it is possible to introduce non-locality in the NN interaction so that it correctly describes the three-nucleon bound states ${}^3\text{H}$ and ${}^3\text{He}$, while still reproducing NN scattering data with high precision. Note that all other NN interactions give a large underbinding of $A \geq 3$ systems. In practice, the INOY interaction was constructed by combining an inner (< 3 fm) phenomenological non-local part with a local Yukawa tail. Hence the name INOY (Inside Non-local Outside Yukawa). The so called IS version of this interaction, introduced in Ref. [26], contains short-range non-local potentials in 1S_0 and ${}^3S_1 - {}^3D_1$ partial waves while higher partial waves are taken from Argonne v_{18} . In this study we are using the IS-M version, which includes non-local potentials also in the P and D waves [25]. It is important to note that, for this particular version, the on-shell properties of the triplet P -wave interactions have been modified in order to improve the description of $3N$ analyzing powers. The 3P_0 interaction was adjusted to become less attractive, the 3P_1 became more repulsive, and the 3P_2 more attractive. Unfortunately, this gives a slightly worse fit to the Nijmegen 3P phase shifts.

III. RESULTS

By construction, the *ab initio* NCSM method is guaranteed to converge either by calculating the effective interaction using a fixed cluster approximation (e.g., two-body) and then solving the eigenvalue problem in increasing model spaces ($N_{\text{max}} \rightarrow \infty$), or by working in a limited model space but increasing the clustering of the effective interaction towards the full A -body one. Our codes are currently constructed to derive effective interactions up to the level of three-body clustering (with or without three-body forces). However, in this study we have chosen to approach convergence by trying to maximize our model space and, therefore, we limit ourselves to the use of two-body effective interactions. Thus we are able to

reach the $9\hbar\Omega$ model space for nuclei with $A = 11$. This maximal space corresponds to basis dimensions of $d_P = 2.0 \times 10^8$ (${}^9\text{Be}$), 7.0×10^8 (${}^{11}\text{Be}$), and 1.1×10^9 (${}^{11}\text{B}$). For ${}^{13}\text{C}$, which is briefly discussed in connection to the parity-inversion problem, the largest space that we were able to reach was $8\hbar\Omega$ ($d_P = 8.2 \times 10^8$).

Note that model spaces with an even(odd) number of HO excitations give negative-(positive-)parity states for the nuclei under study. When constructing a full spectrum we combine the $N_{\text{max}}\hbar\Omega$ and $(N_{\text{max}} + 1)\hbar\Omega$ results, with N_{max} being an even number. In connection to this, we should also point out that very few states in ${}^9\text{Be}$ and ${}^{11}\text{Be}$ are particle stable. However, in the NCSM approach, all states are artificially bound due to the truncated model space and the use of HO basis functions.

In addition to a careful study of the level ordering in ${}^9\text{Be}$ and ${}^{11}\text{Be}$, with a particular focus on the position of the positive-parity states, we also calculate electromagnetic moments and transition strengths. For this we use traditional one-body transition operators with free-nucleon charges. Note that, due to the factorization of our wave function into CM and intrinsic components, we obtain translationally invariant matrix elements for all observables that we investigate in this work. However, we have not renormalized the operators, which means that the results are not corrected for the fact that we work in a truncated model space. The theoretical framework for performing this renormalization is in place, and the process is underway [28]. Until we are ready to implement the use of effective operators, we can get an indication on the need for renormalization by studying the basis-size dependence of our calculated observables.

The cluster decomposition of the ${}^{11}\text{Be}$ ground state into ${}^{10}\text{Be} + n$ is of particular interest due to the small neutron separation energy. We have employed the formalism recently developed in Refs. [20, 21] to calculate cluster overlap functions using our NCSM wave functions. These results are presented in Sec. III C.

A. Dependence on HO frequency

The first step in our study is a search for the optimal HO frequency. In principle, the intrinsic properties of the nucleus should not depend on the particular value of $\hbar\Omega$ since it only enters the Hamiltonian (2) through a CM-dependent term. In practice however, due to the cluster approximation of the effective interaction, our results will be sensitive to the choice of $\hbar\Omega$. Furthermore, by construction, the effective interactions depend on the size of the model space, N_{max} , and on the number of nucleons, A . In order to investigate these dependences we have performed a large series of calculations for a sequence of frequencies. The results from this study are presented in Figs. 1 and 2 (for ${}^9\text{Be}$ and ${}^{11}\text{Be}$, respectively) as curves showing the frequency dependence of the binding energy in different model spaces. We have studied this dependence for the lowest state of each parity. We are look-

ing for the region in which the dependence on Ω is the smallest; and we select this frequency (from the calculation in the largest model space) to use in our detailed investigation of excited states. In our present case, this optimal frequency always corresponds to an energy minimum. Note, however, that the NCSM is not a variational method and the convergence of the binding energy with increasing model space is not always from above.

Following this procedure for each nucleus and interaction, we obtain the optimal HO frequencies that are listed in Table I. A few general remarks regarding the HO dependence, observed for the different interactions in Figs. 1 and 2, can be made: (1) Clear signs of convergence is observed. The dependence on Ω becomes weaker with increasing size of the model space, and the relative difference between the calculated ground-state energies is in general decreasing. Furthermore, the optimal frequencies for the largest model spaces of each parity ($8\hbar\Omega$ and $9\hbar\Omega$) are approximately the same. This motivates our use of a single frequency to compute both positive- and negative-parity states; (2) This single frequency is found to be in the range of about $\hbar\Omega=11\text{--}13$ MeV for all interactions except for INOY, which seems to prefer a significantly larger HO frequency ($\hbar\Omega=16\text{--}17$ MeV); (3) In general, the behavior of the AV8', CDB2k, and N³LO interactions are very similar, but with N³LO having the largest dependence on $\hbar\Omega$; (4) As could be expected, since it is the only *NN* potential which is capable of reproducing *3N* binding energies, the INOY interaction exhibits a distinctively different behavior compared to the three others. The dependence on Ω is encouragingly small, but the ground-state energy is still changing with increasing basis size. This is particularly true for the positive-parity state. We also note, from the insets of Figs. 1 and 2, that it is the only interaction for which the resulting binding energies are approaching the experimental values.

TABLE I: Selected optimal HO frequencies (in [MeV]). These choices are based on the frequency variation studies presented in Figs. 1 and 2.

Nucleus	Interaction			
	INOY	CDB2k	N ³ LO	AV8'
⁹ Be	16	12	11	12
¹¹ Be	17	13	12	12

B. ⁹Be

By studying the HO frequency dependence of the ⁹Be binding energy obtained with different *NN* interactions (see Fig. 1) it is clear that the CDB2k results have a slightly better convergence rate and a weaker HO frequency dependence than AV8' and N³LO. The INOY results display an even weaker frequency dependence, but the binding energy is still moving with increasing N_{max} .

It is clear from Table II that all interactions, with the possible exception of INOY, underbind the system. Actually, by studying the convergence rate of the INOY results in Fig. 1d, it seems as if this interaction will eventually overbind ⁹Be. This observation confirms that the additional binding, usually provided by *3N* forces, can be produced by the INOY interaction. The other three *NN* interactions underbind by 12–14%. The local AV8' potential was also used in a recent GFMC study of negative-parity states in ⁹Be [29], and we find an excellent agreement with their ground-state binding energy (see Table II).

In principle, the frequency dependence for each excited state should be studied in order to compute its energy. This is particularly true in our case where we want to compare negative- and positive-parity states. It is therefore very encouraging that we find the same optimal frequency for the first positive-parity state as for the negative-parity ground state; and we select this frequency to use in our detailed investigation of excited states. In Figs. 3, 4 and Table II we present our NCSM low-energy spectra for different *NN* interactions and compare the results to known experimental levels. As can be seen, the AV8', CDB2k and N³LO interactions give the same level ordering and very similar excitation energies. It is noteworthy that all these high-precision *NN* interactions perform equally when applied to the $A=9$ system. We let the AV8' spectrum shown in Fig. 3 be the graphical representation of all of them. Using the AV8' we can also make a comparison to the recent GFMC calculation [29].

In general, we observe a very reasonable agreement with experimental levels of natural parity, while the unnatural-parity states are consistently high in excitation energy. For both parities, there is a general trend of convergence with increasing model space. When plotting the negative- and positive-parity spectra separately, it is evident that the relative level spacings are almost independent of the model space, so that the level ordering within each parity projection is remarkably stable. It is clear, however, that the relative position of the negative-versus positive-parity states is still not converged. Furthermore, when studying the AV8' convergence pattern in the upper panel of Fig. 3, it seems as if this interaction will predict the positive-parity states at too high excitation energies even when the calculations will be converged. This finding is consistent with an overall trend observed in other NCSM calculations, and it has been speculated whether a three-body force will correct this behavior [16]. Although we are still not able to apply a true three-body force in a large enough model space, we get some indications from the performance of the INOY interaction. In Fig. 4 we see that, for this interaction, the positive-parity states are even higher in small model spaces, but that they are also dropping much faster with increasing N_{max} . This issue is investigated in further detail in Sec. III D where we discuss the important question of parity inversion, and the general trend of the position of natural- versus unnatural-parity states.

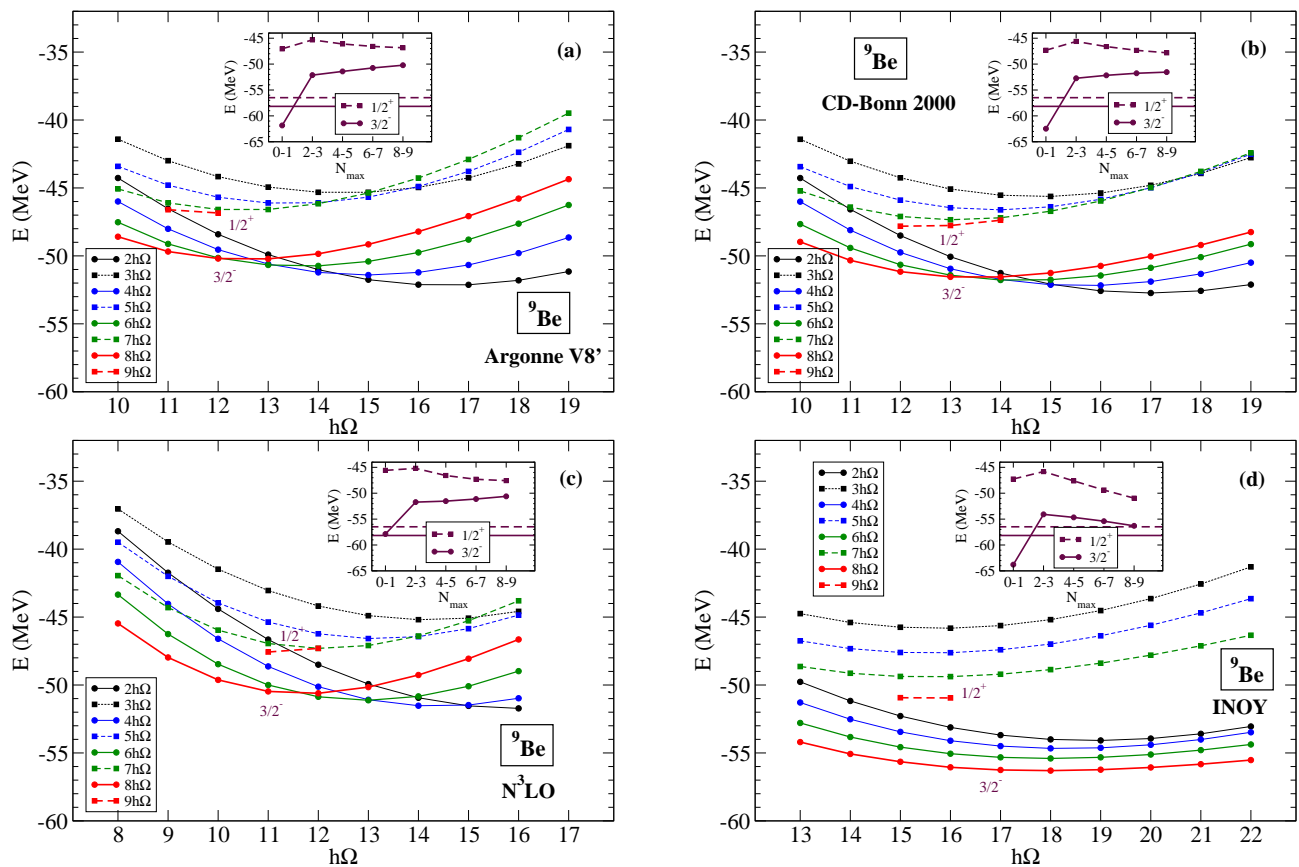


FIG. 1: (Color online) The dependence on HO frequency for the calculated ${}^9\text{Be}(\frac{3}{2}^-, \frac{1}{2}^-)$ (solid lines) and ${}^9\text{Be}(\frac{1}{2}^+, \frac{1}{2}^-)$ (dashed lines) binding energies. Each panel correspond to a particular NN interaction: (a) AV8', (b) CDB2k, (c) $N^3\text{LO}$, (d) INOY; and each separate line corresponds to a specific model space. The insets demonstrate how the minima of the curves converge as the model space is increased. The horizontal lines are the experimental values.

In addition to an increase in binding energy, it has been found that the level ordering for many nuclei can be sensitive to the presence of multi-nucleon forces [29, 30, 31]. This sensitivity is the largest for those states where the spin-orbit interaction strength is known to play a role. For ${}^9\text{Be}$ we find that our calculations with the AV8', CDB2k and $N^3\text{LO}$ interactions predict the first-excited negative-parity state to be a $1/2^-$, while experiments show that it is a $5/2^-$ (Note, however, that the CDB2k interaction predicts these two states to be almost degenerate, and to exhibit a convergence trend indicating a possible level crossing at larger model spaces.). This level reversal was also found in the GFMC calculations using AV8'. The INOY interaction, on the other hand, gives the correct level ordering, but instead overpredicts the spin-orbit splitting. By performing a calculation in a smaller model space using the AV8' plus the Tucson-Melbourne TM'(99) [32] three-nucleon interaction, we found a similar result as with INOY.

Our discussion up to this point has been concentrated on the low-lying levels in ${}^9\text{Be}$. However, in response to the recent evaluation published by the TUNL Nuclear

Data Evaluation Project [33], we have also decided to summarize our results for higher excited states. It is important to note that the experimental widths of these states are generally quite large, and to compute them correctly with the NCSM method requires a very large model space. Furthermore, at high excitation energies, it is very probable that there will be some admixture of $2\hbar\Omega$ intruders, and these are usually predicted too high in the NCSM. In any case, our results can serve as an important guideline as to which p -shell states that can be expected to appear in the spectrum, and consequently should be looked for in experiments. In Table III, we present all levels that we have calculated using the CDB2k interaction in the $8\hbar\Omega$ and $9\hbar\Omega$ model spaces. We also show the tabulated experimental levels below $E_x = 13$ MeV, taken from the most recent evaluation [33]. A quick comparison with the previous, published evaluation [34] (from 1988), reveals that several new levels have been discovered and many spin-parity assignments have been changed. Altogether, these changes lead to a much better agreement with our results. In the negative-parity spectrum, our calculations give the correct level ordering for the first six

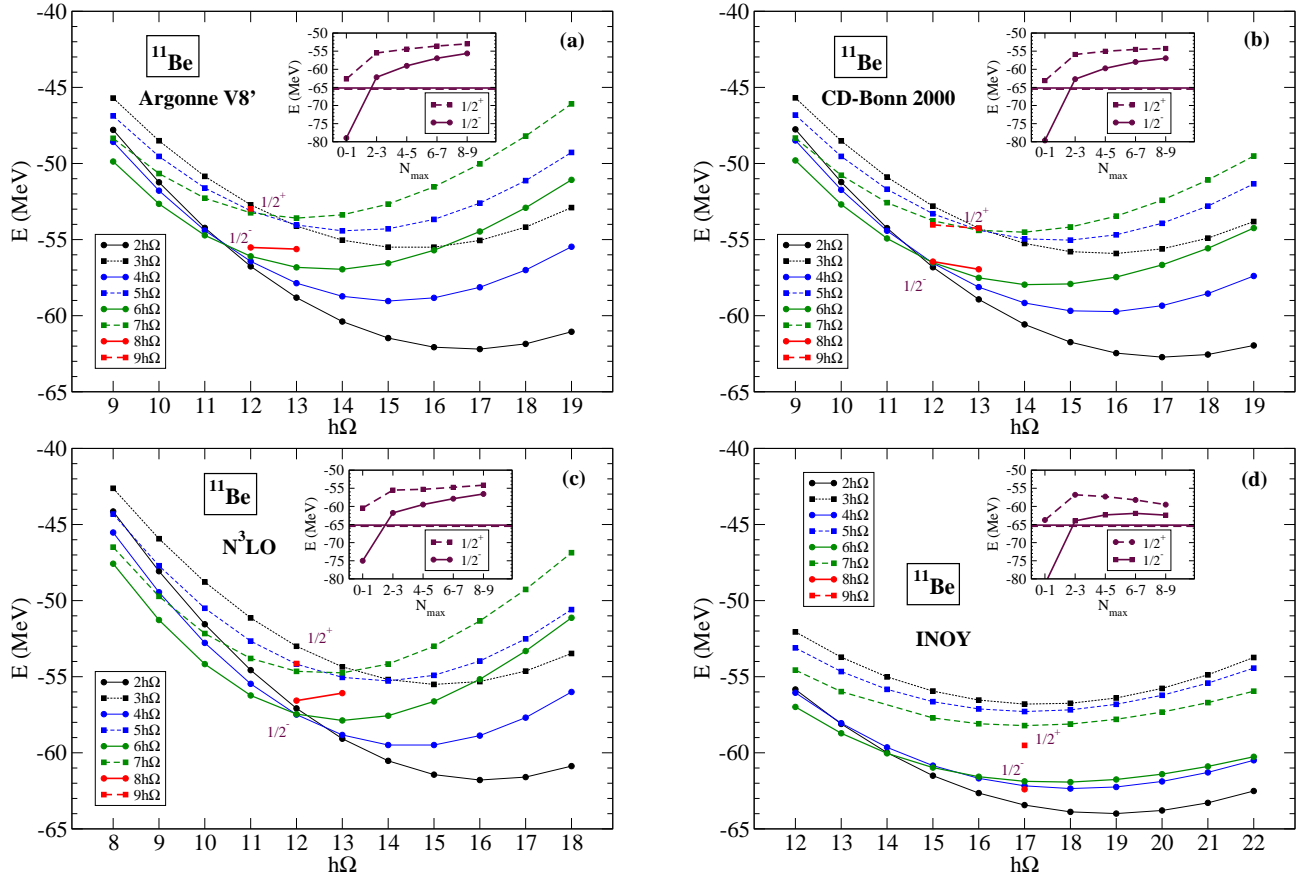


FIG. 2: (Color online) The dependence on HO frequency for the calculated $^{11}\text{Be}\left(\frac{1}{2}_1^- \frac{3}{2}\right)$ (solid lines) and $^{11}\text{Be}\left(\frac{1}{2}_1^+ \frac{3}{2}\right)$ (dashed lines) binding energies. Each panel correspond to a particular NN interaction: (a) AV8', (b) CDB2k, (c) $N^3\text{LO}$, (d) INOY; and each separate line corresponds to a specific model space. The insets demonstrate how the minima of the curves converge as the model space is increased. The horizontal lines are the experimental values.

states. In particular, we correctly reproduce the second $3/2^-$ and $5/2^-$ states that were introduced in the new evaluation. On the other hand, we find a third $3/2^-$ state and a second $1/2^-$ state that have not been observed in experiments. However, these states are not fully converged in our $8\hbar\Omega$ calculation, and they are still moving towards higher excitation energies. We also find a $9/2^-$ state, which is fairly stable, and that has not been experimentally identified. In the positive-parity spectrum, the 6.76 MeV level has now been changed to being a $9/2^+$ which agrees well with our level ordering. Finally, it is interesting to note that our second $1/2^+$, $3/2^+$, and $5/2^+$ levels all appear in between the first $9/2^+$ and $7/2^+$. None of these three states have, however, been experimentally confirmed.

In Table II, we also present our results for the ground-state quadrupole and magnetic moments, as well as for selected electromagnetic transition strengths. We should stress that free-nucleon charges have been used in these calculations, and that the operators have not been renormalized. On the other hand, the stability of our results can be judged by investigating the depen-

dence on the model space. We find that the calculated ground-state magnetic moment and the $B(M1; \frac{5}{2}_1^- \rightarrow \frac{3}{2}_1^-)$ transition strength are almost converged, and in fair agreement with the experimental values. The results for electromagnetic quadrupole observables are, however, steadily increasing with basis size enlargement and should clearly benefit from the use of effective operators. As an example we can consider the evolution of the $N^3\text{LO}$ results: For the $\{4 - 6 - 8\} \hbar\Omega$ sequence of model spaces these observables increase as $Q_{\text{gs}} = \{+3.96 - +4.10 - +4.21\} [efm^2]$, and $B(E2; \frac{5}{2}_1^- \rightarrow \frac{3}{2}_1^-) = \{14.9 - 15.7 - 16.7\} [e^2fm^4]$. We would also like to highlight the fact that INOY gives much smaller values for Q_{gs} and $B(E2)$ than the other interactions. This is partly due to the fact that, for INOY, our selected frequency is much larger than for the other potentials which, in our limited model space, corresponds to a smaller radial scale. In principle, a HO frequency dependence study should be made for each operator. However, we have also applied the INOY interaction in stud-

TABLE II: Experimental and calculated energies (in [MeV]) of the lowest negative- and positive-parity states in ${}^9\text{Be}$. Quadrupole and magnetic moments (in [efm^2] and [μ_N]) for the ground state, as well as E2 and M1 strengths for selected transitions (in [$e^2\text{fm}^4$] and [μ_N^2]). Results for the AV8', CDB2k, N³LO and INOY NN interactions are presented. These calculations were performed in the $8(9)\hbar\Omega$ model space for negative-(positive-)parity states, using the HO frequencies listed in Table I. The GFMC results [29] are shown for comparison. Experimental values are from [33]. E_{x+} denotes the excitation energy relative to the lowest positive-parity state.

${}^9\text{Be}$	NCSM					GFMC
	Exp	INOY	CDB2k	N ³ LO	AV8'	AV8'
$E_{\text{gs}} \left(\frac{3}{2}_1^- \frac{1}{2} \right)$	-58.16	-56.05	-51.16	-50.47	-50.20	-49.9(2)
$E_x \left(\frac{3}{2}_1^- \frac{1}{2} \right)$	0	0	0	0	0	0
$E_x \left(\frac{5}{2}_1^- \frac{1}{2} \right)$	2.43	2.96	2.78	2.64	2.70	2.1
$E_x \left(\frac{1}{2}_1^- \frac{1}{2} \right)$	2.78	4.57	2.68	2.33	2.50	1.7
$E_x \left(\frac{3}{2}_2^- \frac{1}{2} \right)$	5.59 ^a	7.02	4.98	4.53	4.74	—
$E_x \left(\frac{7}{2}_1^- \frac{1}{2} \right)$	6.38	8.09	7.80	7.40	7.56	6.4
$E \left(\frac{1}{2}_1^+ \frac{1}{2} \right)$	-56.48	-50.95	-47.81	-47.57	-46.84	—
$E \left(\frac{1}{2}_1^+ \frac{1}{2} \right) - E_{\text{gs}}$	1.68	5.10	3.35	2.90	3.35	—
$E_{x+} \left(\frac{1}{2}_1^+ \frac{1}{2} \right)$	0	0	0	0	0	—
$E_{x+} \left(\frac{5}{2}_1^+ \frac{1}{2} \right)$	1.37	1.39	1.68	1.68	1.66	—
$E_{x+} \left(\frac{3}{2}_1^+ \frac{1}{2} \right)$	3.02 ^a	4.06	3.60	3.37	3.49	—
$E_{x+} \left(\frac{9}{2}_1^+ \frac{1}{2} \right)$	5.08	6.22	6.36	6.21	6.24	—
Q_{gs}	5.288(38)	3.52	4.01	4.21	4.01	5.0(3)
μ_{gs}	-1.1778(9)	-1.06	-1.22	-1.24	-1.22	-1.35(2)
$B \left(\text{E2}; \frac{5}{2}_1^- \rightarrow \frac{3}{2}_1^- \right)$	27.1(2)	10.9	14.9	16.7	15.0	—
$B \left(\text{M1}; \frac{5}{2}_1^- \rightarrow \frac{3}{2}_1^- \right)$	0.54(6)	0.46	0.37	0.36	0.37	—

^aThe experimental spin-parity assignment of this level is “less certain” according to the TUNL Nuclear Data Evaluation [33].

ies of $A = 3, 4$ systems, for which convergence can be easily reached. It was found that, in particular the rms proton radius is always underpredicted. The same result was obtained in Ref. [35] through exact solutions of the Faddeev-Yakubovskii equations, and it demonstrates that the interaction is too soft, resulting in a faster condensation of nuclear matter. In this work, we have studied the ${}^9\text{Be}$ point-nucleon radii as well as the strong E1 transition from the first-excited to the ground state using the AV8' interaction. However, since these results will be compared to ${}^{11}\text{Be}$ data, we postpone the discussion to Sec. III C.

In Tables IV and V, we show the resulting $N\hbar\Omega$ -configurations and the single-particle occupancies of the ${}^9\text{Be}$ wave function, obtained with the four different interactions. Although these quantities are not physical observables, they can still give interesting information. We see that the wave functions obtained with the AV8', CDB2k and N³LO interactions are almost identical, while the INOY wave function has a considerably larger fraction of low- $\hbar\Omega$ excitations. This fact is in part due to the higher HO frequency being used in the INOY calculations. Furthermore, from Table IV we see that this par-

ticular interaction gives a different distribution of $\hbar\Omega$ excitations for the $\left(\frac{3}{2}_1^- \frac{1}{2} \right)$ and $\left(\frac{1}{2}_1^+ \frac{1}{2} \right)$ states; which would indicate that the latter is slightly more deformed. However, this behavior is not observed for the other interactions. The differences in occupations of single-particle levels reflect some properties of the interactions. The fact that the $0p_{3/2}$ and $0d_{5/2}$ levels have a larger occupation in the INOY eigenstates is direct evidence for a stronger spin-orbit interaction.

C. ${}^{11}\text{Be}$

Most of the observations made for ${}^9\text{Be}$ concerning the frequency dependence of the calculated binding energies also hold true for ${}^{11}\text{Be}$. In general, however, the sensitivity to $\hbar\Omega$ is stronger in the ${}^{11}\text{Be}$ case. Another important remark, that can be made from studying Fig. 2, is that the binding energy of the first positive-parity state calculated with the INOY interaction is clearly not converged. The relative shift in energy is actually slowly increasing with model-space enlargement.

TABLE III: Experimental and calculated energies (in [MeV]) of the lowest negative- and positive-parity states in ${}^9\text{Be}$. The calculations were performed in the $8(9)\hbar\Omega$ model space for negative-(positive-)parity states, using the CDB2k NN interaction with $\hbar\Omega = 12$ MeV. This table represents a more complete compilation of our computed levels (albeit for only one interaction) as compared to Table II. Experimental values are from [33]. E_{x+} denotes the excitation energy relative to the lowest positive-parity state.

Negative parity states ${}^9\text{Be}$			Positive parity states ${}^9\text{Be}$		
	Exp	CDB2k		Exp	CDB2k
E_{gs} $\left(\frac{3}{2}_1^-\right)$	-58.16	-51.16	$E\left(\frac{1}{2}_1^+\right)$	-56.48	-47.81
$E_x\left(\frac{3}{2}_1^-\right)$	0	0	$E\left(\frac{1}{2}_1^+\right) - E_{\text{gs}}$	1.68	3.35
$E_x\left(\frac{5}{2}_1^-\right)$	2.43	2.78	$E_{x+}\left(\frac{1}{2}_1^+\right)$	0	0
$E_x\left(\frac{1}{2}_1^-\right)$	2.78	2.68	$E_{x+}\left(\frac{5}{2}_1^+\right)$	1.37	1.68
$E_x\left(\frac{3}{2}_2^-\right)$	5.59 ^a	4.98	$E_{x+}\left(\frac{3}{2}_1^+\right)$	3.02 ^a	3.60
$E_x\left(\frac{7}{2}_1^-\right)$	6.38	7.80	$E_{x+}\left(\frac{9}{2}_1^+\right)$	5.08	6.36
$E_x\left(\frac{5}{2}_2^-\right)$	7.94 ^a	7.96	$E_{x+}\left(\frac{5}{2}_2^+\right)$		7.66 ^b
$E_x\left(\frac{3}{2}_3^-\right)$		11.26	$E_{x+}\left(\frac{3}{2}_2^+\right)$		7.91 ^b
$E_x\left(\frac{1}{2}_2^-\right)$		11.86	$E_{x+}\left(\frac{1}{2}_2^+\right)$		8.13 ^b
$E_x\left(\frac{9}{2}_1^-\right)$		12.45	$E_{x+}\left(\frac{7}{2}_1^+\right)$		8.48
$E_x\left(\frac{7}{2}_2^-\right)$	11.28 ^a	12.61			
$E_x\left(\frac{5}{2}_3^-\right)$	11.81	13.02			

^aThe experimental spin-parity assignment of this level is “less certain” according to the TUNL Nuclear Data Evaluation [33].

^bCalculated in a smaller, $7\hbar\Omega$, model space.

TABLE IV: Calculated configurations of the first negative- and positive-parity states in ${}^9\text{Be}$. Results obtained in our largest model spaces ($8\hbar\Omega$ and $9\hbar\Omega$, respectively) are presented. The calculations were performed with the HO frequencies listed in Table I.

${}^9\text{Be}\left(\frac{3}{2}_1^-\right)$ ($8\hbar\Omega$ model space)					
NN interaction	$0\hbar\Omega$	$2\hbar\Omega$	$4\hbar\Omega$	$6\hbar\Omega$	$8\hbar\Omega$
INOY	0.58	0.19	0.13	0.06	0.04
CDB2k	0.49	0.22	0.15	0.08	0.06
N ³ LO	0.47	0.24	0.16	0.08	0.06
AV8'	0.49	0.22	0.15	0.08	0.06
${}^9\text{Be}\left(\frac{1}{2}_1^+\right)$ ($9\hbar\Omega$ model space)					
NN interaction	$1\hbar\Omega$	$3\hbar\Omega$	$5\hbar\Omega$	$7\hbar\Omega$	$9\hbar\Omega$
INOY	0.53	0.22	0.14	0.07	0.04
CDB2k	0.48	0.23	0.15	0.08	0.06
N ³ LO	0.46	0.24	0.16	0.08	0.05
AV8'	0.49	0.23	0.15	0.08	0.06

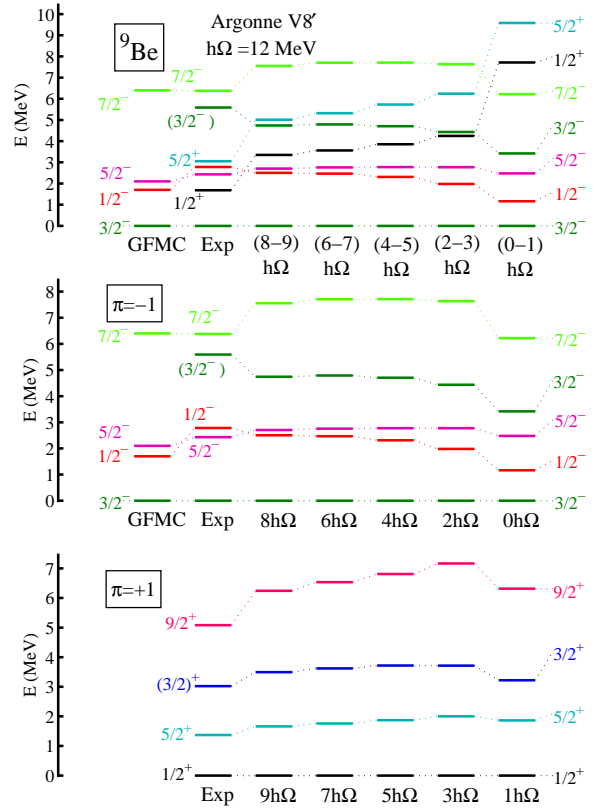


FIG. 3: (Color online) Excitation spectrum for ${}^9\text{Be}$ calculated using the AV8' interaction in $0\hbar\Omega$ – $9\hbar\Omega$ model spaces with a fixed HO frequency of $\hbar\Omega = 12$ MeV. The experimental values are from Ref. [33]. The AV8' results obtained by the GFMC method [29] are shown for comparison (note that only negative-parity states were computed). The two lower graphs show separately the negative- and positive-parity spectra, while the upper graph shows the combined spectrum with selected states.

TABLE V: Calculated occupations of neutron single-particle levels for the first negative- and positive-parity states in ${}^9\text{Be}$. Results obtained in our largest model spaces ($8\hbar\Omega$ and $9\hbar\Omega$, respectively) are presented. The calculations were performed with the HO frequencies listed in Table I.

${}^9\text{Be}\left(\frac{3}{2}_1^-\right)$ ($8\hbar\Omega$ model space)						
NN interaction	$0s_{1/2}$	$0p_{1/2}$	$0p_{3/2}$	$1s_{1/2}$	$0d_{3/2}$	$0d_{5/2}$
INOY	1.804	0.454	2.380	0.043	0.064	0.069
CDB2k	1.773	0.511	2.277	0.067	0.060	0.072
N ³ LO	1.768	0.521	2.256	0.077	0.060	0.072
AV8'	1.778	0.519	2.273	0.064	0.061	0.071
${}^9\text{Be}\left(\frac{1}{2}_1^+\right)$ ($9\hbar\Omega$ model space)						
NN interaction	$0s_{1/2}$	$0p_{1/2}$	$0p_{3/2}$	$1s_{1/2}$	$0d_{3/2}$	$0d_{5/2}$
INOY	1.792	0.498	1.428	0.573	0.111	0.379
CDB2k	1.761	0.530	1.377	0.666	0.113	0.317
N ³ LO	1.757	0.536	1.365	0.676	0.117	0.312
AV8'	1.765	0.535	1.376	0.664	0.113	0.313

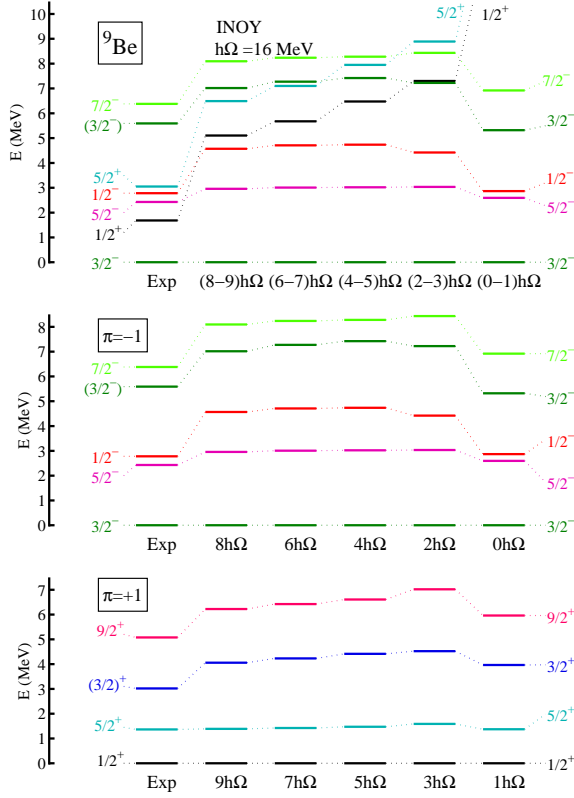


FIG. 4: (Color online) Excitation spectrum for ${}^9\text{Be}$ calculated using the INOY interaction in $0\hbar\Omega$ – $9\hbar\Omega$ model spaces with a fixed HO frequency of $\hbar\Omega = 16$ MeV. The experimental values are from Ref. [33]. The two lower graphs show separately the negative- and positive-parity spectra, while the upper graph shows the combined spectrum with selected states.

The experimental ground state of ${}^{11}\text{Be}$ is an intruder $1/2^+$ level, while the first p -shell state is a $1/2^-$ situated at $E_x = 320$ keV. The neutron separation energy is only 503 keV, and there are no additional bound states. This level-ordering anomaly constitutes the famous parity-inversion problem. A number of excited states have been observed in different reactions and beta-decay studies. However, as can be seen from the summary presented in Table VI, there are considerable ambiguities in the spin-parity assignments.

The low-lying experimental spectrum is compared to our NCSM calculated levels (obtained using the four different NV interactions) in Figs. 5–8 and in Table VII. In the two lower panels of these figures we show, separately, the negative- and positive-parity spectra, while the upper panel shows the combined spectrum with selected states. Note that, those experimental levels for which there is an uncertainty in the parity assignment, are included in all three panels. There are clear signs of convergence with increasing model space. However, as was also observed for ${}^9\text{Be}$, the relative position of the negative- and positive-parity spectra has clearly not converged, and the latter is still moving down. The most

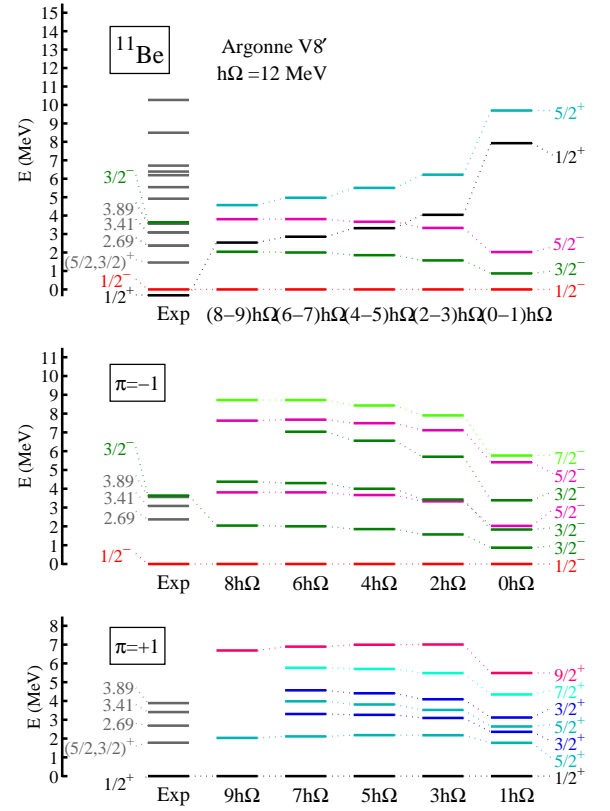


FIG. 5: (Color online) Excitation spectrum for ${}^{11}\text{Be}$ calculated using the AV8' interaction in $0\hbar\Omega$ – $9\hbar\Omega$ model spaces with a fixed HO frequency of $\hbar\Omega = 12$ MeV. The experimental values are from Ref. [39]. The two lower graphs show separately the negative- and positive-parity spectra, while the upper graph shows the combined spectrum with selected states.

dramatic drop is observed in the INOY spectrum, thus indicating the importance of a $3N$ force. With this particular interaction, the $1/2^+$ level actually ends up below all, but one, of the negative-parity states in the $(8-9)\hbar\Omega$ calculation. We refer to Sec. III D for further discussions on this topic.

We stress again that the relative level spacings, observed when plotting negative- and positive-parity states separately, is remarkably stable. Furthermore, the ordering of the first six(four) levels of negative(positive) parity, is the same for all four potentials. This calculated level ordering is summarized in Table VIII. Our results can, therefore, provide input to help resolve the uncertainties of the experimental spin-parity assignments (cf. Table VI). Note in particular that some experiments suggest that there are three low-lying $3/2^-$ states. The task to compute three levels with the same spin quickly becomes very time consuming with increasing dimension, since it requires many Lanczos iterations. Therefore, this third state was studied in two separate runs, using only the AV8' and INOY potentials, and is included in Figs. 5 and 8 up to the $6\hbar\Omega$ model space. These calculations confirm the existence of three low-lying $3/2^-$ levels, but

TABLE VI: Present situation of the spin-parity assignments for the lowest states in ^{11}Be . The table contains published results from the FAS evaluation of 1990 [39] and from more recent experimental studies. These studies include direct reactions such as (t, p) (Liu-Fortune) and $^{12}\text{C}(^{11}\text{Be}, ^{11}\text{Be}')$ (Fukuda) in which the extracted angular distributions were analyzed using DWBA theory. The remaining references are measurements of β -delayed neutrons in coincidence with γ -rays. All decays that were observed in these experiments had $\log(ft)$ values that were consistent with allowed transitions, indicating that the corresponding final states have negative parity and $J \leq \frac{5}{2}$.

Ref.	States (MeV)								
	0.0	0.32	1.78	2.69	3.41	3.89	3.96	5.24	5.86
Ajz.-Sel. [39]	$\frac{1}{2}^+$	$\frac{1}{2}^-$	$(\frac{5}{2}, \frac{3}{2})^+$	$(\frac{1}{2}, \frac{3}{2}, \frac{5}{2})^+$	$(\frac{1}{2}, \frac{3}{2}, \frac{5}{2})^+$	$\geq \frac{7}{2}$	$\frac{3}{2}^-$		
Liu [36]	$\frac{1}{2}^+$	$\frac{1}{2}^-$	$\frac{5}{2}^+$	$\frac{3}{2}^-$	$\frac{3}{2}^-$	$\frac{3}{2}^+$	$\frac{3}{2}^-$	$\frac{5}{2}^-$	$(\frac{1}{2}^+, \frac{1}{2}^-)$
Morrisey [47]	$\frac{1}{2}^+$	$\frac{1}{2}^-$	(+)	(-)	(+)	(-)	(-)	(-)	(-)
Aoi [37]	$\frac{1}{2}^+$	$\frac{1}{2}^-$	$\frac{5}{2}^+$	$\frac{3}{2}^-$	$\frac{3}{2}^-$	$\frac{3}{2}^+$	$\frac{3}{2}^-$	$\frac{5}{2}^-$	
Hirayama [38]	$\frac{1}{2}^+$	$\frac{1}{2}^-$	(+)	$\frac{3}{2}^-$	$\frac{3}{2}^-$	$\frac{3}{2}^+$	$\frac{3}{2}^-$	$\frac{5}{2}^-$	
Fukuda [48]	$\frac{1}{2}^+$	$\frac{1}{2}^-$	$(\frac{3}{2}, \frac{5}{2})^+$		$(\frac{3}{2}, \frac{5}{2})^+$				

TABLE VII: Experimental and calculated energies (in [MeV]) of the lowest negative- and positive-parity states in ^{11}Be , as well as the magnetic moment (in [μ_N]) of the ground state. Results for the AV8', CDB2k, N³LO and INOY NN interactions are presented. These calculations were performed in the $8(9)\hbar\Omega$ model space for negative-(positive-)parity states, using the HO frequencies listed in Table I. E_{x-} denotes the excitation energy relative to the lowest negative-parity state. Experimental values are from [39, 42].

^{11}Be	NCSM				
	Exp	INOY	CDB2k	N ³ LO	AV8'
$E \left(\frac{1}{2}_1^- \frac{3}{2} \right)$	-65.16	-62.40	-56.95	-56.57	-55.52
$E \left(\frac{1}{2}_1^- \frac{3}{2} \right) - E_{\text{gs}}$	0.32	-2.89	-2.69	-2.44	-2.54
$E_{x-} \left(\frac{1}{2}_1^- \frac{3}{2} \right)$	0	0	0	0	0
$E_{x-} \left(\frac{3}{2}_1^- \frac{3}{2} \right)$? ^a	2.99	2.27	2.08	2.04
$E_{x-} \left(\frac{5}{2}_1^- \frac{3}{2} \right)$? ^a	3.82	3.93	3.70	3.81
$E_{x-} \left(\frac{3}{2}_2^- \frac{3}{2} \right)$? ^a	6.93	4.91	4.43	4.38
$E_{\text{gs}} \left(\frac{1}{2}_1^+ \frac{3}{2} \right)$	-65.48	-59.51	-54.26	-54.13	-52.98
$E_x \left(\frac{1}{2}_1^+ \frac{3}{2} \right)$	0	0	0	0	0
$E_x \left(\frac{5}{2}_1^+ \frac{3}{2} \right)$? ^a	1.85	2.01	1.98	2.03
μ_{gs}	-1.6816(8)	-1.47	-1.55	-1.58	-1.58

^aThere are large ambiguities in the experimental spin-parity assignments, cf. Table VI

TABLE VIII: NCSM observed ordering (from left to right) of ^{11}Be negative- and positive-parity states (separately). Note that all four NN interactions used in this study give the same ordering for the first six(four) negative-(positive-)parity states.

Negative parity					
$\frac{1}{2}^-$	$\frac{3}{2}^-$	$\frac{5}{2}^-$	$\frac{3}{2}^-$	$\frac{3}{2}^-$	$\frac{5}{2}^-$
Positive parity					
$\frac{1}{2}^+$	$\frac{5}{2}^+$	$\frac{3}{2}^+$	$\frac{5}{2}^+$		

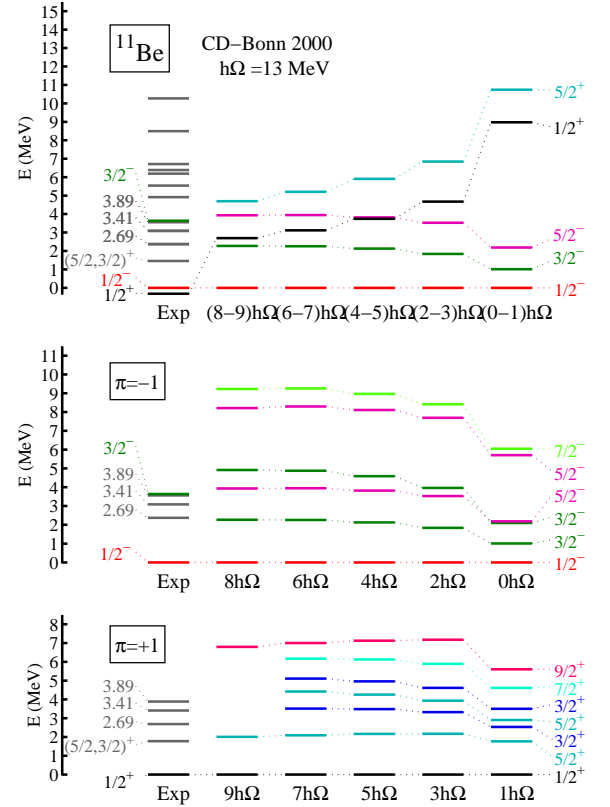


FIG. 6: (Color online) Excitation spectrum for ^{11}Be calculated using the CDB2k interaction in $0\hbar\Omega-9\hbar\Omega$ model spaces with a fixed HO frequency of $\hbar\Omega = 13$ MeV. The experimental values are from Ref. [39]. The two lower graphs show separately the negative- and positive-parity spectra, while the upper graph shows the combined spectrum with selected states.

they also stress the presence of a $5/2^-$ state which is not completely consistent with Refs. [36, 37, 38]. However, we can not rule out the possibility of a low-lying intruder $2\hbar\Omega$ -dominated state, which would avoid detection in our study. These states have a different convergence pat-

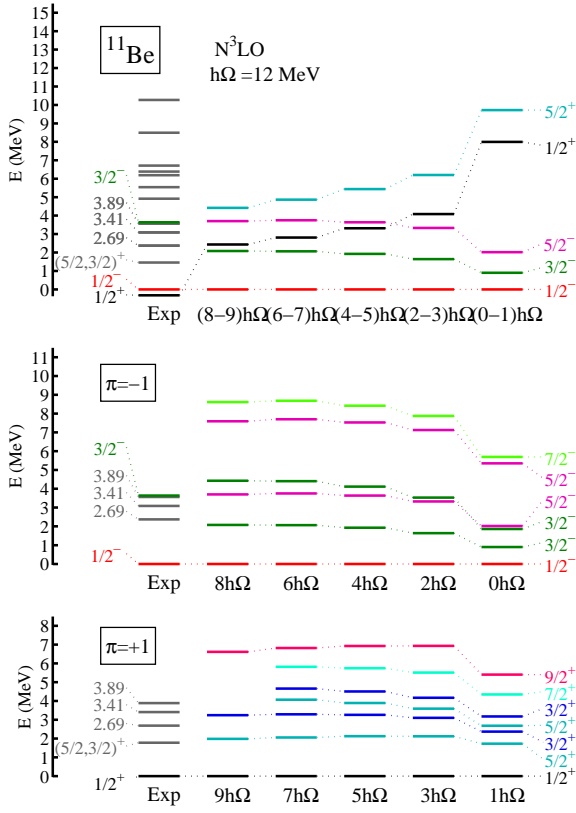


FIG. 7: (Color online) Excitation spectrum for ^{11}Be calculated using the $N^3\text{LO}$ interaction in $0\hbar\Omega$ – $9\hbar\Omega$ model spaces with a fixed HO frequency of $\hbar\Omega = 12$ MeV. The experimental values are from Ref. [39]. The two lower graphs show separately the negative- and positive-parity spectra, while the upper graph shows the combined spectrum with selected states.

tern than $0\hbar\Omega$ states and generally appear at too high an excitation energy in the smaller model spaces, see e.g. Ref. [19].

In summary, our results suggest that there are two excited positive-parity states below 4 MeV (rather than three as stated in Ref. [39]). The 1.78 MeV level should be a $5/2^+$ state, while either the 3.41 or the 3.89 MeV level is a $3/2^+$. Our results do not support the presence of a high-spin ($J \geq 7/2$) state, which one can find in Ref. [39]. We do observe three low-lying $3/2^-$ states although they are accompanied by a $5/2^-$ state.

The strength of the electric dipole transition between the two bound states in ^{11}Be is of fundamental importance. This is an observable which has attracted much attention since it was first measured in 1971 [40], and again in 1983 [41]. The cited value of 0.36 W.u. is still the strongest known transition between low-lying states, and it has been attributed to the halo character of the bound-state wave functions. Unfortunately, by working in a HO basis, we suffer from an incorrect description of the long-range asymptotics, and we would need an extremely large number of basis states in order to reproduce the correct form. This shortcoming of the HO

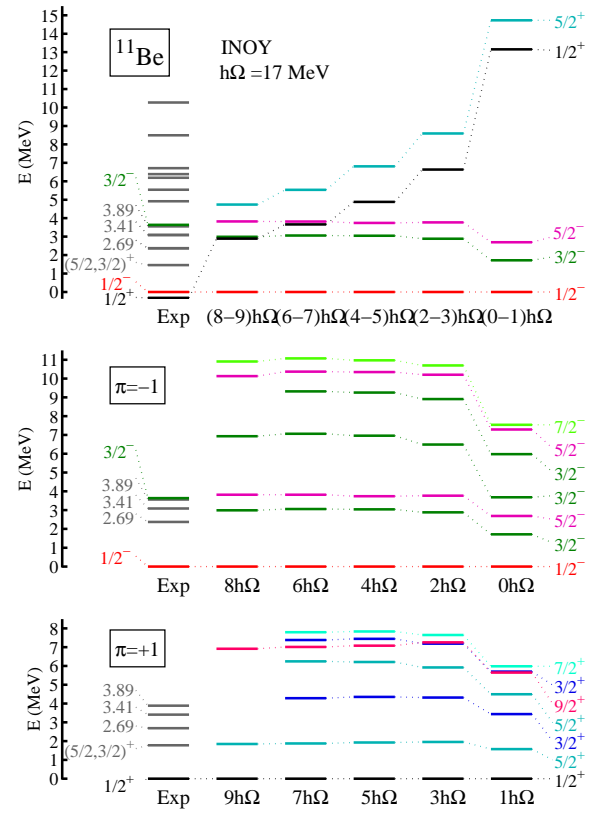


FIG. 8: (Color online) Excitation spectrum for ^{11}Be calculated using the INOY interaction in $0\hbar\Omega$ – $9\hbar\Omega$ model spaces with a fixed HO frequency of $\hbar\Omega = 17$ MeV. The experimental values are from Ref. [39]. The two lower graphs show separately the negative- and positive-parity spectra, while the upper graph shows the combined spectrum with selected states.

basis is illustrated by the fact that we obtain a value for the E1 strength which is 20 times too small (see Table IX). When studying the dependence of this value on the size of the model space, we observe an almost linear increase, indicating that our result is far from converged. For the $\{(4-5) - (6-7) - (8-9)\}$ $\hbar\Omega$ sequence of model spaces, the ^{11}Be E1 strength, $B\left(E1; \frac{1}{2}_1^+ \rightarrow \frac{1}{2}_1^+\right)$, calculated with the AV8' interaction increases as: $\{0.0054 - 0.0059 - 0.0065\} [e^2\text{fm}^2]$. The corresponding sequence of results for ^9Be is: $B\left(E1; \frac{1}{2}_1^+ \rightarrow \frac{3}{2}_1^-\right) = \{0.029 - 0.031 - 0.033\} [e^2\text{fm}^2]$, which demonstrates a similar increase. However, for this nucleus we note that, in the largest model space, our calculated E1 strength is only off by a factor of two compared to experiment. In addition, a consistent result is found for the much weaker $\frac{5}{2}_1^+ \rightarrow \frac{3}{2}_1^-$ E1 transition in ^9Be , where we also obtain a factor of two smaller $B(E1)$ than experiment. These results accentuates the anomalous strength observed for ^{11}Be . A simple explanation for the failure of HO calculations in the ^{11}Be case was given by Millener *et al* [41]. It was shown that there is a strong cancellation in the cal-

culated E1 transition amplitude due to the insufficient description of the long-range asymptotics (see in particular Tables IV and V in Ref. [41]). By simply replacing their HO single-particle wave functions with solutions to the Schrödinger equation with a Woods-Saxon potential, they found that the magnitude of the neutron $1s_{1/2}0p_{1/2}$ single-particle matrix element increased significantly so that the cancellation was removed. Even though our multi- $\hbar\Omega$ calculations give a significant improvement of the calculated E1 strengths as compared to their simple $(0-1)\hbar\Omega$ model, the underlying problem is still present.

Another operator which is sensitive to the long-range behavior of the wave function is the point-nucleon radius. However, even though no operator renormalization has been applied, our results show a fair stability with increasing model space, and they are in rather good agreement with experimental findings for both ^9Be and ^{11}Be (see Table IX). It is probably safe to assume that the missing part of the ^{11}Be matter radius originates mainly in an underestimation of the point-neutron radius. One should also remember that the experimental results for matter radii, in these light systems, are highly model-dependent and are usually theoretically extracted from measurements of the interaction cross section. In addition, we have also calculated the radii of the first excited state. For both isotopes it is found that the unnatural-parity state has a 10% larger neutron radius than the natural-parity one, probably due to a larger admixture of sd -shell neutrons. Finally, the ground-state magnetic moment of ^{11}Be has been measured [42] and we find a reasonable agreement with our calculated value, see Table VII.

TABLE IX: Nuclear ground-state radii (in [fm]) and the E1 strengths (in [$e^2\text{fm}^2$]) for the strong ground-state transitions in ^9Be and ^{11}Be . The NCSM calculations were performed in the $8(9)\hbar\Omega$ model space for negative-(positive-)parity states using the AV $8'$ interaction. The GFMC result for ^9Be , with the same interaction [29], is shown for comparison. Experimental values are from [33, 39, 49, 50].

$^9\text{Be}\left(\frac{3}{2}_1^-\frac{1}{2}\right)$					
	R_n	R_p	R_{mat}	$B(\text{E1})$	
				$\frac{1}{2}_1^+ \rightarrow \frac{3}{2}_1^-$	$\frac{5}{2}_1^+ \rightarrow \frac{3}{2}_1^-$
Exp		2.39	2.45(1) ^a	0.061(25)	0.0100(84)
NCSM	2.40	2.27	2.34	0.033	0.0057
GFMC	—	2.41(1)	—	—	—
$^{11}\text{Be}\left(\frac{1}{2}_1^+\frac{3}{2}\right)$					
	R_n	R_p	R_{mat}	$B(\text{E1})$	
				$\frac{1}{2}_1^- \rightarrow \frac{1}{2}_1^+$	
Exp			2.86(4)	0.116(12)	
NCSM	2.66	2.30	2.54	0.0065	

^aInteraction radius

The standard halo picture of the ^{11}Be ground state is a simple two-body configuration consisting of an inert ^{10}Be core coupled to an $s_{1/2}$ valence neutron. Theoret-

ical estimates of the spectroscopic factor for this component range from 0.55 to 0.92, see e.g. Table 1 in Ref. [43]. The experimental situation is also unclear since the extracted results are generally model-dependent. In the literature one can find values from 0.36 to 0.8, see e.g. Fig. 8 in Ref. [44]. An important question is to which extent the first-excited $^{10}\text{Be}(2_1^+)$ state contributes to the simple two-body configuration. The formalism for investigating cluster structures of NCSM eigenstates was recently developed in Ref. [21]. We have calculated the overlap of the $^{11}\text{Be}\left(\frac{1}{2}_1^+\frac{3}{2}\right)$ state with different $^{10}\text{Be} + n$ channels. To this aim, the $^{11}\text{Be}(^{10}\text{Be})$ wave functions were calculated using the CDB2k interaction in a $7(6)\hbar\Omega$ model space. We used a HO frequency of $\hbar\Omega = 14$ MeV, which corresponds to the optimal value for calculating binding energies in these two model spaces. The largest overlap functions (in jj coupling) are presented in Fig. 9, while the corresponding spectroscopic factors (the overlap function squared and integrated over all r) are summarized in Table X. Several additional channels, such as the overlap with the second excited 2_2^+ state in ^{10}Be , were also computed but their spectroscopic factors were found to be very small ($\lesssim 0.001$).

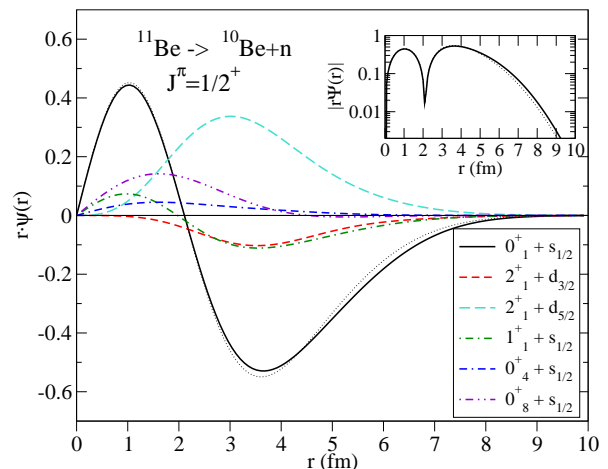


FIG. 9: (Color online) The largest radial overlap functions for the $^{11}\text{Be}\left(\frac{1}{2}_1^+\frac{3}{2}\right)$ state decomposed as $^{10}\text{Be} + n$ in jj -coupling. The results presented here were obtained with the CDB2k interaction ($\hbar\Omega = 14$ MeV) with the $^{11}\text{Be}(^{10}\text{Be})$ wave function calculated in a $7(6)\hbar\Omega$ model space. The thin, dotted line shows the dominant overlap function calculated in a smaller $5(4)\hbar\Omega$ model space.

Several observations can be made when studying these results: (1) The ^{11}Be ground state has a large overlap with [$^{10}\text{Be}(0_1^+) \otimes n(s_{1/2})$] ($S = 0.82$), but also with the core-excited [$^{10}\text{Be}(2_1^+) \otimes n(d_{5/2})$] channel ($S = 0.26$). These results are in good agreement with the consensus of recent experimental studies, see e.g. Refs. [43, 45]. (2) The thin dotted line in Fig. 9 shows the [$^{10}\text{Be}(0_1^+) \otimes n(s_{1/2})$] overlap function calculated in a smaller model space. From this comparison it is clear that the results are quite

TABLE X: Spectroscopic factors for the ^{11}Be ($\frac{1}{2}_1^+ \frac{3}{2}$) ground state decomposed as $^{10}\text{Be} + n$ in jj coupling. The results presented here were obtained with the CDB2k interaction ($\hbar\Omega = 14$ MeV) with the ^{11}Be (^{10}Be) wave function calculated in a $7(6)\hbar\Omega$ model space. For comparison, we list spectroscopic factors extracted from three recent experiments utilizing different reactions.

$^{10}\text{Be} \otimes n$		Transfer	Knockout	Breakup	
J^π	(l, j)	NCSM	[43] ^a	[45] ^b	[44] ^c
0_1^+	$(0, \frac{1}{2})$	0.818	0.67-0.80	0.78	0.61(5), 0.77(4)
2_1^+	$(2, \frac{3}{2})$	0.263	0.09-0.16		
2_1^+	$(2, \frac{5}{2})$	0.022			
1_1^+	$(0, \frac{3}{2})$	0.032			
0_4^+	$(0, \frac{1}{2})$	0.005			
0_8^+	$(0, \frac{1}{2})$	0.037			

^aDWBA analysis of $^{11}\text{Be}(p, d)$.

^bFrom ^9Be ($^{11}\text{Be}, ^{10}\text{Be} + \gamma$)

^cSpectroscopic factors extracted from ^{11}Be breakup on lead and carbon targets respectively.

stable with regards to a change in N_{max} . The interior part does hardly change at all, while the tail is slowly extending towards larger inter-cluster distances. This statement is true for all channels shown in the figure except for those involving the two high-lying 0^+ states [see bullet (4) below]. (3) The inset shows the main component plotted on a logarithmic scale. This graph clearly demonstrates the fact that our HO basis is not large enough to reproduce the correct asymptotic behavior. Even though the tail is extending further with increasing N_{max} , it still does not reach the expected exponential decay. Instead it dies of too fast. (4) Our calculated ^{10}Be 0_4^+ and 0_8^+ states are found to be $2\hbar\Omega$ dominated, and their binding energies have not converged in the NCSM calculation. The cluster overlaps with these states do not display the same stability as observed for the other channels. Instead, there is a large dependence on N_{max} . A similar result was found in Ref. [21] and it is just another manifestation of the slower convergence of the $2\hbar\Omega$ states in the NCSM.

Finally, we compare, in Tables XI and XII, the resulting configurations and the occupancies of single-particle states obtained with different interactions. Again, it is clear that the INOY eigenstates have a larger fraction of low- $\hbar\Omega$ excitations and that this interaction results in a different single-particle spectrum due, most likely, to a stronger spin-orbit interaction.

D. Parity inversion

One of the main objectives of this study has been to investigate the relative position of negative- and positive-parity states in the region around ^{11}Be . As we have shown, none of our calculations reproduce the parity inversion that is observed for this nucleus. However, con-

TABLE XI: Calculated configurations of the first negative- and positive-parity states in ^{11}Be . Results obtained in our largest model spaces ($8\hbar\Omega$ and $9\hbar\Omega$, respectively) are presented. The calculations were performed with the HO frequencies listed in Table I.

$^{11}\text{Be}(\frac{1}{2}_1^- \frac{3}{2})$ ($8\hbar\Omega$ model space)					
NV interaction	$0\hbar\Omega$	$2\hbar\Omega$	$4\hbar\Omega$	$6\hbar\Omega$	$8\hbar\Omega$
INOY	0.59	0.17	0.14	0.06	0.04
CDB2k	0.51	0.20	0.15	0.08	0.06
N ³ LO	0.49	0.22	0.15	0.08	0.06
AV8'	0.48	0.21	0.16	0.08	0.07
$^{11}\text{Be}(\frac{1}{2}_1^+ \frac{3}{2})$ ($9\hbar\Omega$ model space)					
NV interaction	$1\hbar\Omega$	$3\hbar\Omega$	$5\hbar\Omega$	$7\hbar\Omega$	$9\hbar\Omega$
INOY	0.56	0.20	0.14	0.06	0.04
CDB2k	0.50	0.21	0.15	0.08	0.06
N ³ LO	0.49	0.22	0.16	0.08	0.06
AV8'	0.48	0.22	0.16	0.08	0.07

TABLE XII: Calculated occupations of neutron single-particle levels for the first negative- and positive-parity states in ^{11}Be . Results obtained in our largest model spaces ($8\hbar\Omega$ and $9\hbar\Omega$, respectively) are presented. The calculations were performed with the HO frequencies listed in Table I.

$^{11}\text{Be}(\frac{1}{2}_1^- \frac{3}{2})$ ($8\hbar\Omega$ model space)						
NV interaction	$0s_{1/2}$	$0p_{1/2}$	$0p_{3/2}$	$1s_{1/2}$	$0d_{3/2}$	$0d_{5/2}$
INOY	1.862	1.078	3.643	0.046	0.065	0.075
CDB2k	1.835	1.093	3.597	0.066	0.062	0.072
N ³ LO	1.832	1.095	3.586	0.073	0.062	0.072
AV8'	1.828	1.094	3.579	0.073	0.061	0.072
$^{11}\text{Be}(\frac{1}{2}_1^+ \frac{3}{2})$ ($9\hbar\Omega$ model space)						
NV interaction	$0s_{1/2}$	$0p_{1/2}$	$0p_{3/2}$	$1s_{1/2}$	$0d_{3/2}$	$0d_{5/2}$
INOY	1.845	0.504	3.300	0.658	0.086	0.345
CDB2k	1.824	0.600	3.181	0.742	0.088	0.285
N ³ LO	1.823	0.616	3.153	0.752	0.091	0.281
AV8'	1.820	0.630	3.135	0.768	0.088	0.265

sidering the slower convergence rate for $1\hbar\Omega$ -dominated states in the NCSM, and the large, but still finite, model spaces that we were able to use, our results are actually very promising. In all nuclei, we found a fast drop of the unnatural-parity states with respect to the natural ones. This behavior has already been demonstrated in earlier NCSM studies, but the drop that we observe in ^{11}Be is the most dramatic so far. Furthermore, the results obtained with the INOY interaction are clearly different from the others, which indicates the significance that a realistic $3N$ force should have in a fundamental explanation of the parity inversion. Note that INOY is a two-body interaction, but that it simulates the main effects of $3N$ forces by short-range, non-local terms. Furthermore, the 3P NV interactions are slightly modified in order to improve the description of $3N$ an-

alyzing powers. Fig. 10 shows the calculated excitation energy of the first positive-parity states in ${}^9\text{Be}$ and ${}^{11}\text{Be}$ as a function of the basis size, N_{max} . For illustrative purposes we have extrapolated our results to larger model spaces assuming an exponential dependence on N_{max} , i.e., $E_x = E_{x,\infty} + a \exp(-bN_{\text{max}})$. Note that the $(0-1)\hbar\Omega$ points are excluded from the fits. The extrapolated

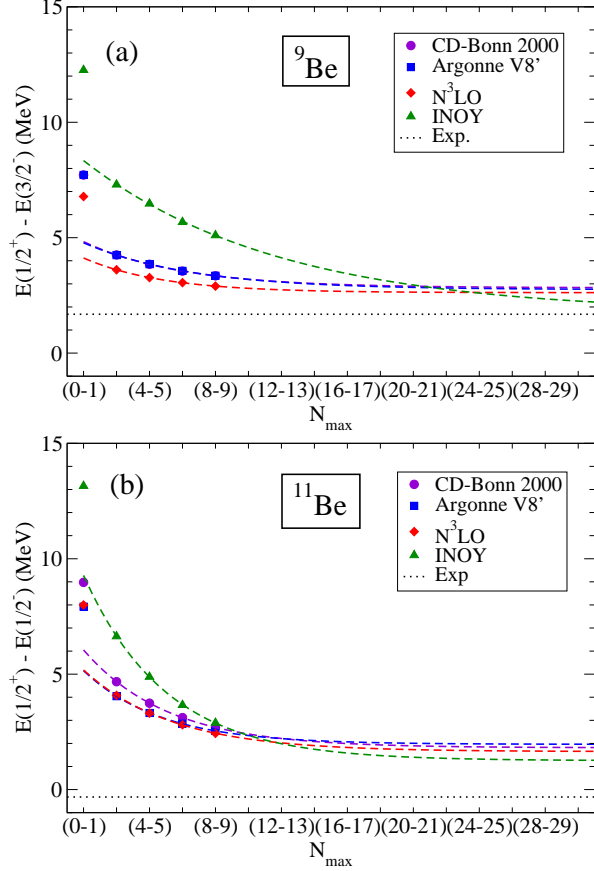


FIG. 10: (Color online) Basis size dependence of the calculated $E_x\left(\frac{1}{2}^+\right)$ excitation energy relative to the lowest negative-parity state in (a) ${}^9\text{Be}$ and (b) ${}^{11}\text{Be}$. The results for four different NN interactions are compared. For each potential, a single, fixed HO frequency was used (see Table I). The dashed lines correspond to exponential fits of the calculated data and, for illustration, these curves are extrapolated to larger model spaces.

INOY results end up below the other interactions; and for ${}^9\text{Be}$ the curve is actually approaching the experimental value. With all other interactions, the extrapolated excitation energy is $\approx 1-2$ MeV too high.

When discussing the position of the first unnatural-parity state, it is very interesting to study the systematics within the $A = 11$ isobar and the $N = 7$ isotope. To this aim, we have performed large-basis calculations for ${}^{11}\text{B}$ and ${}^{13}\text{C}$. The diagonalization of the ${}^{11}\text{B}$ Hamiltonian in the $9\hbar\Omega$ space proved to be our largest calculation so far. For ${}^{13}\text{C}$ we were only able to reach the $8\hbar\Omega$ space. Both studies were performed us-

ing the CDB2k interaction and an HO frequency of $\hbar\Omega = 13$ MeV. The ground-state binding energies (obtained in the $8\hbar\Omega$ space) are: $E\left({}^{11}\text{B}; \frac{3}{2}^- \frac{1}{2}\right) = 66.25$ MeV, and $E\left({}^{13}\text{C}; \frac{1}{2}^- \frac{1}{2}\right) = 86.53$ MeV. Our calculated ${}^{11}\text{B}$ spectrum, including the first negative-parity state for each spin up to $J = 9/2$, plus the lowest positive-parity state, is compared to known experimental levels in Fig. 11. Note that we obtain an incorrect $1/2^-$ ground-state spin in our largest model space. However, the first $3/2^-$ and $1/2^-$ states are found to be almost degenerate, and there is a trend indicating that the position of these levels may eventually intersect as the basis size is increased. In principle, a thorough frequency variation study should be performed in order to clarify the fine details of the predictions. In any case, it is clear that the level splitting is described incorrectly with this interaction. Basically the same result was found in an earlier NCSM study [31] using a three-body effective interaction derived from AV8'. In that paper, it was also shown that the correct level ordering can be reproduced, and the splitting greatly improved, by adding a realistic $3N$ force. For ${}^{13}\text{C}$ we have only computed the lowest state for each parity. However, this nucleus has also been studied previously using the NCSM. A spectrum obtained with the CDB2k interaction was presented in Ref. [46], while calculations with a genuine $3N$ force were reported in Ref. [31]. In both papers, the study was limited to negative-parity states and a smaller model space ($4\hbar\Omega$) was used.

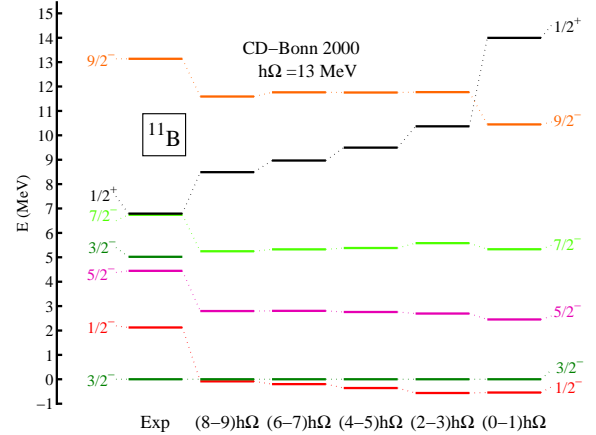


FIG. 11: (Color online) Excitation spectrum for ${}^{11}\text{B}$ calculated using the CDB2k interaction in $0\hbar\Omega-9\hbar\Omega$ model spaces with a fixed HO frequency of $\hbar\Omega = 13$ MeV. The experimental levels are from Ref. [39]. Note that there are many additional levels between the experimental $1/2^+$ and $9/2^-$ shown in the figure. However, we have only computed the first level for a given spin, and the $1/2^+$ was the only positive-parity state that was considered.

Let us now comment on our ${}^{11}\text{B}$ and ${}^{13}\text{C}$ results and return to the important question of the position of the first positive-parity state. The calculated $1/2^+$ excitation energy for these two nuclei, as a function of N_{max} , is

shown in Fig. 12. It is a fascinating empirical fact that, by simply going from $Z = 4 \rightarrow Z = 6$, the first $1/2^+$ state moves from being the ground state in ^{11}Be to become an excited state at 3.1 MeV in ^{13}C . In the odd- Z nucleus ^{11}B , the first positive-parity state is found quite high in the excitation spectrum, namely at 6.8 MeV. It is a significant success of the NCSM method, and of the NN interactions being employed, that these huge shifts are accurately reproduced in our calculations. However, as can be seen from Figs. 10 and 12, the calculated excitation energy always turns out to be too large. A comparison of our extrapolated CDB2k results shows that they exceed the experimental values by $\approx 1-2$ MeV for all four isotopes. As a final remark, our INOY results for ^9Be and ^{11}Be indicate that the use of a realistic $3N$ force in a large basis space might correct this discrepancy.

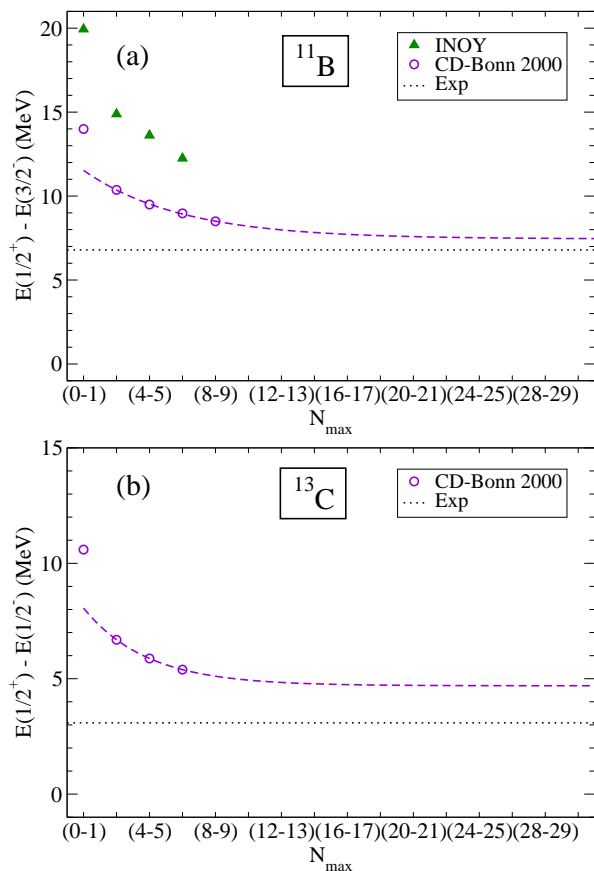


FIG. 12: (Color online) Basis size dependence of the calculated $E_x\left(\frac{1}{2}^+\right)$ excitation energy relative to the lowest negative-parity state in (a) ^{11}B and (b) ^{13}C . These results are obtained with the CDB2k interaction and $\hbar\Omega = 13$ MeV. The dashed lines correspond to exponential fits of the calculated data and, for illustration, these curves are extrapolated to larger model spaces.

IV. CONCLUSIONS

We have performed large-basis *ab initio* no-core shell model calculations for ^9Be and ^{11}Be using four different realistic NN interactions. One of these, the non-local INOY interaction, has never before been used in nuclear structure calculations. Although it is formally a two-body potential, it reproduces not only NN data (beware of the fact that the 3P interactions are slightly modified in the IS-M version that we are using) but also the binding energies of ^3H and ^3He . Therefore it has been of particular interest for our current application, where we have striven to maximize the model space by limiting ourselves to NN interactions, but have still been very much interested in the effects of three-body forces. We have computed: binding energies, excited states of both parities, electromagnetic moments and transition strengths, point-nucleon radii, and also the core-plus-neutron cluster decomposition of the ^{11}Be ground state.

In summary, for the calculated spectra we found clear signs of convergence, and a remarkable agreement between the predictions of different NN interactions. In particular, the relative level spacings observed when plotting positive- and negative-parity states separately, were found to be very stable and to agree well with experimental spectra. This has allowed us to make some conclusions regarding the largely unknown spin-parities of unbound, excited states in ^{11}Be . An overall observation is that the AV8' and $N^3\text{LO}$ potentials produce very similar results, while CDB2k gives slightly more binding. The INOY interaction is clearly different; giving a much larger binding energy and a stronger spin-orbit splitting. Both these effects would be expected from a true $3N$ force, but are here achieved by the use of short-range, non-local terms in the NN interaction.

Furthermore, it was also clear from our study that our results for observables connected to long-range operators, have not converged. These calculations would clearly benefit from operator renormalization, in order to correct for the limited model space being used. In particular, the extremely strong E1 transition between the two bound states in ^{11}Be , was underestimated by a factor of 20. We have discussed how this illustrates the fact that the anomalous strength is due to the halo character, and hence large overlap, of the initial and final state wave functions; a property which is extremely hard to reproduce using a HO basis. In the NCSM approach, there is no fitting to single-particle properties, e.g., by the use of empirical interactions. Instead, the effective interactions are derived from the underlying inter-nucleon forces. Therefore, it is likely that a good description of loosely bound, and unbound, single-particle states might require a very large number of HO basis functions.

An important topic of this work has been the investigation of the parity inversion found in ^{11}Be . We did not reproduce the anomalous $1/2^+$ ground state in our *ab initio* approach, but did observe a dramatic drop of the positive-parity excitation energies with increasing model

space. Furthermore, the behavior of our INOY results suggests that a realistic $3N$ force will have an important influence on the parity inversion. However, in order to pursue this question further, an improved computational capacity is needed. We have also performed large-basis calculations for ^{11}B and ^{13}C . In this way, we were able to put our ^{11}Be positive-parity results into a wider context by studying the systematics within the $Z = 4$ isotopes (^9Be), the $N = 7$ isotone (^{13}C), and the $A = 11$ isobar (^{11}B). Although we found that the NCSM always overestimates the excitation energy of the first unnatural-parity state, we did reproduce the very large shifts observed for these different nuclei. This is an important finding which leads us to the optimistic conclusion that the parity-inversion problem should be possible to repro-

duce in the NCSM starting from realistic inter-nucleon interactions.

Acknowledgments

This work was partly performed under the auspices of the U. S. Department of Energy by the University of California, Lawrence Livermore National Laboratory under contract No. W-7405-Eng-48. Support from the LDRD contract No. 04-ERD-058, and from U.S. Department of Energy, Office of Science, (Work Proposal Number SCW0498) is acknowledged.

-
- [1] I. Talmi and I. Unna, *Phys. Rev. Lett.* **4**(9), 469 (1960).
 [2] D. J. Millener, *Nucl. Phys. A* **693**, 394 (2001).
 [3] W. D. Teeters and D. Kurath, *Nucl. Phys. A* **275**, 61 (1977).
 [4] T. Otsuka, N. Fukunishi, and H. Sagawa, *Phys. Rev. Lett.* **70**(10), 1385 (1993).
 [5] H. Esbensen, B. A. Brown, and H. Sagawa, *Phys. Rev. C* **51**(3), 1274 (1995).
 [6] F. M. Nunes, I. J. Thompson, and R. C. Johnson, *Nucl. Phys. A* **596**, 171 (1996).
 [7] A. Doté and H. Horiuchi, *Prog. Theor. Phys.* **103**(1), 91 (2000).
 [8] Y. Kanada-En'yo and H. Horiuchi, *Phys. Rev. C* **66**, 024305 (2002).
 [9] K. Arai, Y. Ogawa, Y. Suzuki, and K. Varga, *Phys. Rev. C* **54**(1), 132 (1996).
 [10] P. Descouvemont, *Nucl. Phys. A* **699**, 463 (2002).
 [11] B. S. Pudliner, V. R. Pandharipande, J. Carlson, S. C. Pieper, and R. B. Wiringa, *Phys. Rev. C* **56**, 1720 (1997).
 [12] P. Navrátil, J. P. Vary, and B. R. Barrett, *Phys. Rev. Lett.* **84**(25), 5728 (2000).
 [13] P. Navrátil, J. P. Vary, and B. R. Barrett, *Phys. Rev. C* **62**, 054311 (2000).
 [14] K. Suzuki and S. Y. Lee, *Prog. Theor. Phys.* **64**, 2091 (1980).
 [15] K. Suzuki, *Prog. Theor. Phys.* **68**(1), 246 (1982).
 [16] E. Caurier, P. Navrátil, W. E. Ormand, and J. P. Vary, *Phys. Rev. C* **66**, 024314 (2002).
 [17] E. Caurier and F. Nowacki, *Acta Phys. Pol. B* **30**(3), 705 (1999).
 [18] E. Caurier, G. Martínez-Pinedo, F. Nowacki, A. Poves, J. Retamosa, and A. P. Zuker, *Phys. Rev. C* **59**, 2033 (1999).
 [19] E. Caurier, P. Navrátil, W. E. Ormand, and J. P. Vary, *Phys. Rev. C* **64**, 051301(R) (2001).
 [20] P. Navratil, *Phys. Rev. C* **70**, 014317 (2004).
 [21] P. Navratil, *Phys. Rev. C* **70**, 054324 (2004).
 [22] R. B. Wiringa, V. G. J. Stoks, and R. Schiavilla, *Phys. Rev. C* **51**, 38 (1995).
 [23] R. Machleidt, *Phys. Rev. C* **63**, 024001 (2001).
 [24] D. R. Entem and R. Machleidt, *Phys. Rev. C* **68**, 041001(R) (2003).
 [25] P. Doleschall, *Phys. Rev. C* **69**, 054001 (2004).
 [26] P. Doleschall, I. Borbély, Z. Papp, and W. Plessas, *Phys. Rev. C* **67**, 0064005 (2003).
 [27] P. Navrátil and E. Caurier, *Phys. Rev. C* **69**, 014311 (2004).
 [28] I. Stetcu, B. R. Barrett, P. Navrátil, and C. W. Johnson, *nucl-th/0409072*.
 [29] S. C. Pieper, K. Varga, and R. B. Wiringa, *Phys. Rev. C* **66**, 044310 (2002).
 [30] P. Navrátil and W. E. Ormand, *Phys. Rev. Lett.* **88**(15), 152502 (2002).
 [31] P. Navrátil and W. E. Ormand, *Phys. Rev. C* **68**, 034305 (2003).
 [32] S. A. Coon and H. K. Han, *Few-Body Syst.* **30**(1-2), 131 (2001).
 [33] D. R. Tilley, J. H. Kelley, J. L. Godwin, D. J. Millener, J. E. Purcell, C. G. Sheu, and H. R. Weller, *Nucl. Phys. A* **745**, 155 (2004).
 [34] F. Ajzenberg-Selove, *Nucl. Phys. A* **490**, 1 (1988).
 [35] R. Lazauskas and J. Carbonell, *Phys. Rev. C* **70**, 044002 (2004).
 [36] G.-B. Liu and H. T. Fortune, *Phys. Rev. C* **42**, 167 (1990).
 [37] N. Aoi, K. Yoneda, H. Miyatake, H. Ogawa, Y. Yamamoto, E. Ideguchi, T. Kishida, T. Nakamura, M. Notani, H. Sakurai, et al., *Nucl. Phys. A* **616**, 181c (1997).
 [38] Y. Hirayama, T. Shimoda, H. Izumi, H. Yano, M. Yagi, A. Hatakeyama, C. D. P. Levy, K. P. Jackson, and H. Miyatake, *Nucl. Phys. A* **738**, 201 (2004).
 [39] F. Ajzenberg-Selove, *Nucl. Phys. A* **506**, 1 (1990), *Energy levels of light nuclei A=11* (April 2004 revised manuscript). Available WWW: http://www.tunl.duke.edu/nuclldata/fas/11_1990.pdf.
 [40] K. Hanna, S. S. and Nagatani, W. R. Harris, and J. W. Olness, *Phys. Rev. C* **3**, 2198 (1971).
 [41] D. J. Millener, J. W. Olness, E. K. Warburton, and S. S. Hanna, *Phys. Rev. C* **28**, 497 (1983).
 [42] W. Geithner, S. Kappertz, M. Keim, P. Lievens, R. Neugart, L. Vermeeren, S. Wilbert, V. N. Fedoseyev, U. Köster, V. I. Mishin, et al., *Phys. Rev. Lett.* **83**(19), 3792 (1999).
 [43] J. S. Winfield, S. Fortier, W. N. Catford, S. Pita, N. A. Orr, J. Van de Wiele, Y. Blumenfeld, R. Chapman, S. P. G. Chappell, N. M. Clarke, et al., *Nucl. Phys. A*

- 683**, 48 (2001).
- [44] R. Palit, P. Adrich, T. Aumann, K. Boretzky, B. V. Carlson, D. Cortina, U. D. Pramanik, T. W. Elze, H. Emling, H. Geissel, et al., *Phys. Rev. C* **68**, 034318 (2003).
- [45] T. Aumann, A. Navin, D. P. Balamuth, D. Bazin, B. Blank, J. A. Brown, J. E. Bush, J. A. Caggiano, B. Davids, T. Glasmacher, et al., *Phys. Rev. Lett.* **84**(1), 35 (2000).
- [46] G. Thiamová, V. Burjan, J. Cejpek, V. Kroha, and P. Navrátil, *Nucl. Phys. A* **697**, 25 (2002).
- [47] D. J. Morrissey, K. N. McDonald, D. Bazin, B. A. Brown, R. Harkewicz, N. A. Orr, B. M. Sherrill, G. A. Souliotis, M. Steiner, J. A. Winger, et al., *Nucl. Phys. A* **627**, 222 (1997).
- [48] N. Fukuda, T. Nakamura, N. Aoi, N. Imai, M. Ishihara, T. Kobayashi, H. Iwasaki, T. Kubo, A. Mengoni, M. Notani, et al., *Phys. Rev. C* **70**, 054606 (2004).
- [49] I. Tanihata, T. Kobayashi, O. Yamakawa, S. Shimoura, K. Ekuni, K. Sugimoto, N. Takahashi, T. Shimoda, and H. Sato, *Phys. Lett. B* **206**(4), 592 (1988).
- [50] G. Fricke, C. Bernhardt, K. Heilig, L. A. Schaller, L. Schellenberg, E. B. Shera, and C. W. De Jager, *At. Data Nucl. Data Tables* **60**(2), 177 (1995).